ADVANCED MATERIALS
www.advmat.de

Reprogramming Mitochondrial Metabolism in Synovial Macrophages of Early Osteoarthritis by a Camouflaged Meta-Defensome

Lei Zhang, Xiang Chen, Pingqiang Cai, Han Sun, Siyu Shen, Baosheng Guo,* and Qing Jiang**

Osteoarthritis (OA) is a low-grade inflammatory and progressive joint disease, and its progression is closely associated with an imbalance in M1/M2 synovial macrophages. Repolarizing pro-inflammatory M1 macrophages into the anti-inflammatory M2 phenotype is emerging as a strategy to alleviate OA progression but is compromised by unsatisfactory efficiency. In this study, the reprogramming of mitochondrial dysfunction is pioneered with a camouflaged meta-Defensome, which can transform M1 synovial macrophages into the M2 phenotype with a high efficiency of 82.3%. The meta-Defensome recognizes activated macrophages via receptor–ligand interactions and accumulates in the mitochondria through electrostatic attractions. These meta-Defensomes are macrophage-membrane-coated polymeric nanoparticles decorated with dual ligands and co-loaded with S-methylisothiourea and MnO_2. Meta-Defensomes are demonstrated to successfully reprogram the mitochondrial metabolism of M1 macrophages by scavenging mitochondrial reactive oxygen species and inhibiting mitochondrial NO synthase, thereby increasing mitochondrial transcription factor A expression and restoring aerobic respiration. Furthermore, meta-Defensomes are intravenously injected into collagenase-induced osteoarthritis mice and effectively suppress synovial inflammation and progression of early OA, as evident from the Osteoarthritis Research Society International score. Therefore, reprogramming the mitochondrial metabolism can serve as a novel and practical approach to repolarize M1 synovial macrophages. The camouflaged meta-Defensomes are a promising therapeutic agent for impeding OA progression in tclinic.

1. Introduction

Osteoarthritis (OA) is a progressive degenerative joint disease characterized by articular cartilage destruction and synovial inflammation.[1] Pathological changes in joints can lead to progressive functional limitations and joint dysfunction, thereby disrupting the quality of life.[2] Reports indicated that this is the primary cause of disability worldwide and is an enormous clinical and economic burden.[3] There is growing evidence showing that inflammation (particularly synovitis) is significantly associated with OA severity (except for mechanical loading), which indicates a major role of innate immunity in OA progression.[4] However, clinical therapeutics for OA treatments only relieve pains and symptoms. Their therapeutic effects are tremendously limited by poor bioavailability, low stability, and rapid joint clearance.[5] Given the complicated pathogenesis of OA in the end stage, joint replacement has been the single choice to cease disease progression,[6] which is, unfortunately, confronted with high costs and high risks of surgical failures for OA patients.[7] Hence, there is an urgent need to develop novel therapeutic agents to manage and prevent early-stage OA.

Lines of evidence have demonstrated that synovial macrophages play a critical role in the symptomology and structural progression of OA.[8] Macrophages are generally dichotomized into two phenotypes: pro-inflammatory M1 and anti-inflammatory M2. An imbalance in M1/M2 synovial macrophages was highly correlated with OA severity.[9] M2 macrophages secrete anti-inflammatory cytokines associated with the resolution of inflammation.[10] In contrast, M1 macrophages are predominant during the early stage of inflammation and secrete pro-inflammatory cytokines such as interleukin (IL)-1β and tumour necrosis factor (TNF)-α. Notably, activated M1 macrophages produce reactive oxygen species (ROS) and nitric oxide (NO), resulting in 30-fold higher amounts of NO than in the M2 phenotype.[11] In line with this, current therapeutic agents are designed to regulate intracellular ROS and NO levels, attempting to repolarize M1 into M2 macrophages.[12] However, these attempts involve intermittent

L. Zhang, X. Chen, P. Cai, H. Sun, S. Shen, B. Guo, Q. Jiang
State Key Laboratory of Pharmaceutical Biotechnology
Division of Sports Medicine and Adult Reconstructive Surgery
Department of Orthopedic Surgery
Nanjing Drum Tower Hospital
The Affiliated Hospital of Nanjing University Medical School
Branch of National Clinical Research Center for Orthopedics
Sports Medicine and Rehabilitation
321 Zhongshan Road, Nanjing, Jiangsu 210008, P. R. China
E-mail: pqcai@nju.edu.cn; borisguo@nju.edu.cn; qingj@nju.edu.cn
P. Cai
Chemistry and Biomedicine Innovation Center
Nanjing University
Nanjing 210093, P. R. China
The ORCID identification number(s) for the author(s) of this article can be found under https://doi.org/10.1002/adma.202202715.

DOI: 10.1002/adma.202202715

and prolonged drug administration (over 4 weeks) due to insufficient M1 macrophage repolarization (less than 50%).[13] It is probably because the mitochondria-derived ROS and NO that account for 90% of the ROS and NO production have not yet been resolved.[14]

Therefore, it is necessary to resolve mitochondrial metabolism and its relationship with M1/M2 imbalance in OA. Previous studies have established that the energy metabolic pathways of M1 macrophages differ from those of their M2 counterparts in tumors, showing disordered mitochondrial respiration.[15] M1 macrophages in tumors exhibit high levels of inducible nitric oxide synthase (iNOS) and hydrogen peroxide (H_2O_2),[11b,16] which increases NO competing with oxygen (O_2) for cytochrome c oxidase, resulting in mitochondrial dysfunction and increased mitochondrial reactive oxygen species (mtROS). This abnormal metabolic pathway in M1 macrophages aggravates oxidative stress and elevates the secretion of inflammatory factors, contributing to the development of tumors.[17] It has been reported that mitochondrial dysfunction and oxidative stress contribute to dysregulation of the inflammatory response.[18] Inflammatory M1 macrophage activation blunts oxidative phosphorylation, thereby preventing repolarization.[19] In addition, mitochondrial ROS plays a key role in promoting macrophage polarization to inflammatory M1 phenotype in inflammation-related diseases.[12d,20] Therefore, therapeutically restoring mitochondrial function might be useful to improve the reprogramming of inflammatory M1 macrophages into anti-inflammatory M2 cells to control the disease. In tumor-associated macrophages, the modulation of the mitochondrial morphology results in T-cell activation and enhances anti-tumor immunity.[21] Meanwhile, reprogramming of macrophages from M1 to M2 can be achieved by targeting rescue mitochondria metabolism.[22] Unfortunately, mitochondrial metabolism in synovial macrophages in OA remains unclear. Reprogramming mitochondria might be able to repolarize synovial macrophages from M1 to M2 phenotypes, if mitochondrial dysfunction accounts for the M1/M2 imbalance in OA.[23] So far, there has been no effective strategy to repolarize M1 macrophages by restoring mitochondrial dysfunction.

Biomaterial-based inflammation control has recently gained much attention in the treatment of arthritis.[24] Biomaterials can be applied to targeted delivery of anti-inflammatory therapeutics to desired cells, tissues, and organs, to anti-inflammatory efficacy, and to reduce toxicity.[24a] Among them, membrane-coated nanocarriers inherit the biological functionalities of the source cells, such as superior biocompatibility, long circulation time, and disease-relevant targeting ability; and therefore have been widely used in inflammation-related diseases. Recently, red blood cells (RBCs) and platelets have been exploited as membrane materials for concealing nanoparticles.[25] Nonetheless, nonhomologous RBCs and platelet membranes can cause abnormal or heterogeneous immune responses in vivo.[26] In addition, the low content of functional biomolecules on membranes limits their targeting capabilities when wrapping functionalized nanoparticles.[27] By contrast, immunocyte membranes are emerging as novel camouflages for introducing nanomedicine formulations into the immune system, such as cell membranes originating from macrophages, NK cells, T-cells, and dendritic cells.[28] Among them, membranes from NK cells, T-cells, and dendritic cells are advantageous in activating innate and adaptive immune responses and are therefore widely used in immunotherapies for cancer elimination.[29] However, the pathogenesis of OA, including biomechanical and metabolic factors, is complex and restricts its use in OA treatment.[30] Many studies have shown that nanocarriers, cloaked in the macrophage membrane providing a camouflage effect, can evade immunological surveillance.[31] Macrophage membrane-coated nanocarriers have exhibited high targeting efficiency in various inflammatory diseases, including rheumatoid arthritis, cancer, and sepsis.[32] In addition, macrophage membrane-coated nanocarriers are rendered with prolonged circulation. Despite the camouflage effect, it is necessary to further boost the phagocytosis of warped nanocarriers through a bio-friendly strategy.[32] It is indispensable to engineer the macrophage membrane, to promote the entry of wrapped nanocarriers into synovial macrophages, and repolarize the M1 phenotype into the M2 phenotype.

Here, we hypothesized that such innate chemotaxis towards inflammation might promote the accumulation of drug-loaded macrophage mimics in the inflammatory tissues of OA joints, thereby defending them against worsening inflammation. Hence, we developed a novel meta-Defensome by metabolically engineering macrophage membrane coated PLGA nanoparticles (MMP) to target M1 macrophages and selectively release cargoes in the mitochondria. The meta-Defensomes were further camouflaged with dual-targeting ligands, by decorating the wrapping membrane with dextran sulfate (DS) by MGE-mediated bioorthogonal copper-free click chemistry,[33] and DSPE-PEG_{2000}-TPP[34] through post-insertion techniques. It could regulate mitochondrial metabolism and promote M2 macrophage transformation in OA models by efficient scavenging of mtROS and inhibition of NO production locally in mitochondria (**Figure 1**). In the meta-Defensome, manganese dioxide nanoparticles (MnO_2 NPs, 5 nm) were encapsulated to scavenge abnormal mtROS, which effectively triggered the decomposition of H_2O_2 and release of oxygen. S-methylisothiourea (SMT), an iNOS inhibitor, was simultaneously incorporated to inhibit abnormal mtNOS expression. The obtained meta-Defensomes were shown to successfully target the synovitis site of OA joints after intravenous injection in response to inflammatory factors, restore mitochondrial dysfunction in M1 macrophages, and drive macrophage polarization from M1 to M2 phenotype via regulating the expression of mitochondrial transcription factor A (TFAM). Camouflaged meta-Defensomes targeted activated macrophages at synovitis from OA mice at an early stage in response to inflammatory factors and effectively recognized M1 macrophages by targeting the SRA receptor, thereby achieving real-time visualization by bimodal MRI/IVIS imaging. Notably, camouflaged meta-Defensomes effectively attenuate oxidative stress and suppress inflammation in the OA synovium to prevent OA progression through regulating the mitochondrial dysfunction of M1 synovial macrophages in collagenase-induced osteoarthritis (CIOA) mice. Therefore, our study demonstrates a promising therapeutic strategy to effectively prevent OA progression via the targeted interface of mitochondria metabolism, which has excellent potential for clinical OA treatment.

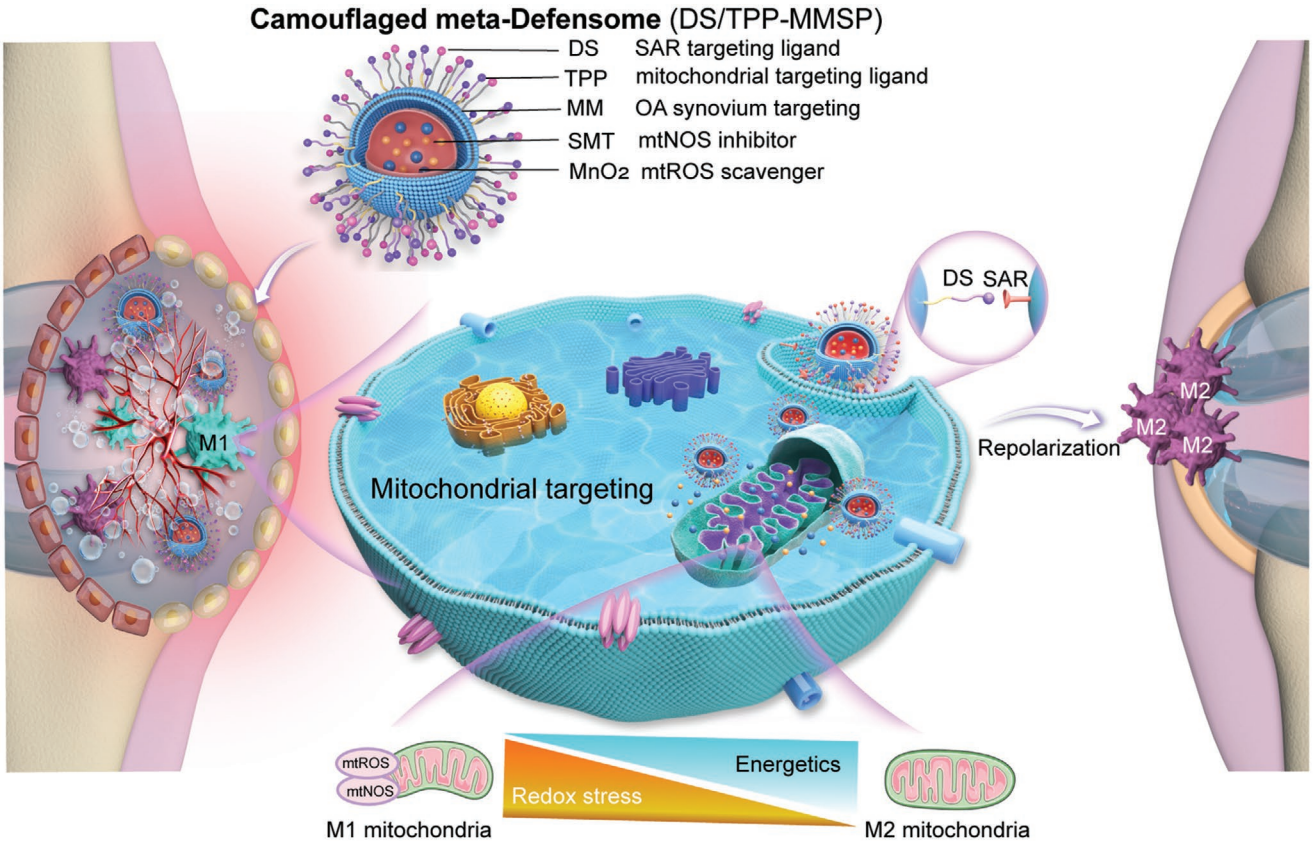

Figure 1. Schematic of targeted mitochondrial metabolism reprogramming in M1 synovial macrophages. The meta-Defensome (DS/TPP-MMSP) targeted the synovitis site of OA joints after systemic administration and specifically accumulated in the mitochondria of M1 macrophages. Subsequently, meta-Defensomes reprogramed pro-inflammatory M1 macrophages to the anti-inflammatory M2 phenotype by restoring aerobic respiration. The reprogramming is achieved through scavenging mtROS and inhibiting mtNOS which both increase TFAM expression.

2. Results and Discussion

2.1. Mitochondrial Dysfunction is Positively Associated with OA Severity

Synovial macrophages play a critical role in the pathogenesis of OA. The ratio of M1/M2 phenotypes of synovial macrophages is known to increase with OA severity, and thus there exists a perturbation of homeostasis.[35] This suggests that reprogramming M1 macrophages into the M2 subtype might be a promising therapeutic option for OA treatment. To find an effective reprogramming strategy, we performed single-cell RNA sequencing of the human synovium to investigate the abnormal gene expression of synovial macrophages in OA patients. As shown in the t-SNE analysis (**Figure 2**A), three transcriptionally distinct macrophage clusters were identified in the synovium of healthy controls and patients with OA. In the human OA synovium, M0 macrophages were activated into M1 and M2 phenotypes, which led to enhanced synovial hyperplasia and macrophage-related synovial inflammation as shown by the hematoxylin and eosin (H&E) staining (Figure S1, Supporting Information). In addition, the ratio of M1/M2 macrophage in the human OA synovium was 4.8-fold higher than that in the normal synovium, which is consistent with previous studies.[35b,36] The OA synovium exhibited more iNOS-positive cells (marking M1 macrophages) than the normal synovium, as well as a 3.8-fold increase in scavenger receptor class A (SRA) (Figure S2, Supporting Information). In contrast, the number of CD206-positive cells in the OA synovium was significantly lower than that of iNOS-positive cells, suggesting an imbalance in the M1/M2 ratio (Figure S2A, Supporting Information). Meanwhile, the human OA synovium showed higher levels of inflammatory cytokines (TNF-α and IL-1β) than the normal synovium (Figure S3, Supporting Information), which is consistent with the proportion of M1 cells.

To screen the genes associated with increased M1 polarization, we analyzed differentially expressed genes for each cluster and chose upregulated and downregulated genes (log2 FC $\geq$ 0.36 and p-value $\leq$ 0.01) in human OA synovium by the likelihood-ratio test. The expression heatmap showed dozens of genes associated with mitochondrial dysfunction were downregulated in M1 macrophages (Figure 2B). Many of these genes are essential for the maintenance of mitochondrial biogenesis and energy production, including MT-CO3,[37] MTATP6P1,[38] MT-ATP6,[39] MT-CYB,[40] MT-ND4,[41] RNR2,[42] and MT-DN1.[43] Moreover, MT-ND3[44] and MT-CO3[37,45] can be regulated by hypoxia, and their dysfunction is related to oxidative stress, oxygen supply, and lipid metabolism (Figure 2C, Figure S4, Supporting Information). This implies that mitochondrial dysfunction might contribute to the vastly increased number

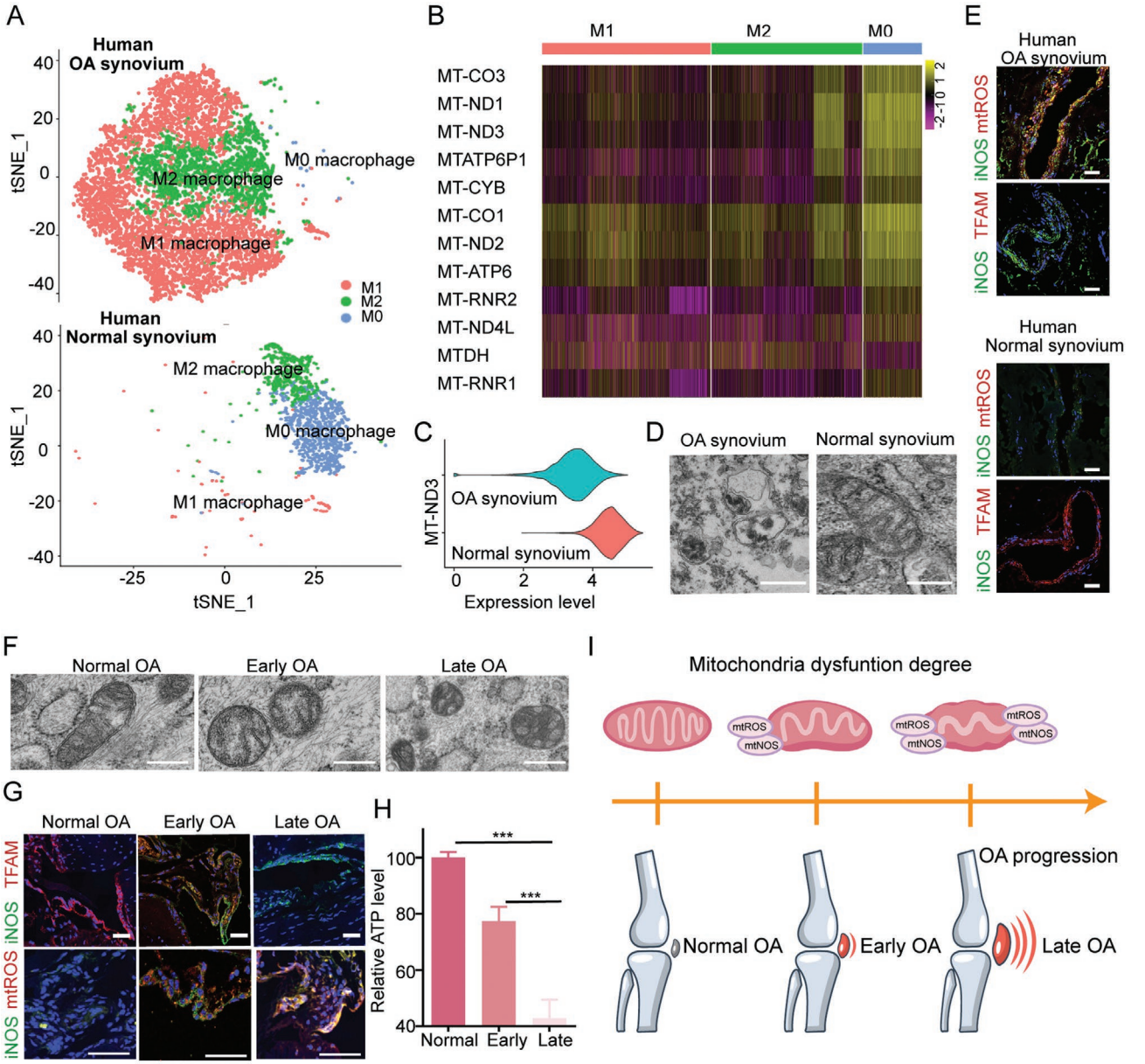

Figure 2. Mitochondrial dysfunction in M1 synovial macrophages promoted the progression of human OA. A) 2D t-SNE visualization of 8796 cells in synovium from normal patients ($n = 3$) and OA patients ($n = 3$). Three transcriptionally distinct macrophage clusters (M0, M1, and M2) were identified. The ratio of M1 macrophage in OA synovial tissues was 4.8-fold higher than in normal tissues. B) Heatmap of differentially expressed genes in macrophage clusters from synovial tissues ($n = 3$) in (A). Columns show differentially expressed signature genes in each cluster, and rows exhibited different clusters (M0, M1, and M2). C) Violin plots showing the differential expression of MT-ND3 in each cluster of M1 macrophages in the synovium from OA patients ($n = 3$) and healthy subjects ($n = 3$). Mitochondrial biogenesis-related gene MT-CO3 and Hypoxia-related gene MT-ND3 were downregulated in OA synovium compared to normal ones. D) TEM images of mitochondria in OA and normal human synovium. Mitochondria in OA human synovium were swollen, and round-shaped, and the mitochondrial cristae were disrupted, whereas mitochondria in normal human synovium were less swollen with well-organized cristae. Scale bars: 500 nm. E) Immunofluorescence imaging of iNOS/mtROS (top) and iNOS/TFAM (bottom) in OA and normal human synovium. The mtROS level (red) and TFAM expression (red) were investigated in M1 macrophages (cells stained positively for iNOS (green)). M1 macrophage from OA synovium exhibited severe mitochondrial damage, as evident from the increased mtROS levels, and the decreased TFAM expression. Scale bars: 50 µm. F) TEM images of mitochondria in the synovium from normal, early CIOA, and late CIOA mice models. The damage to mitochondrial integrity was positively correlated with OA severity. Scale bars: 500 nm. G) Immunofluorescence imaging of iNOS / TFAM and iNOS/mtROS in the synovium from normal, early CIOA, and late CIOA mice models. The mtROS level (Red) and TFAM expression (red) were investigated in M1 macrophages (cells stained positively for iNOS (green)). M1 mitochondrial dysfunction marker is positively correlated with OA severity. Scale bars: 50 µm. The upregulated mtROS level and downregulated TFAM expression in M1 macrophages positively correlate with OA severity. H) Bar chart showing ATP levels in synovium from normal and CIOA mice with early or late stage. The downregulated ATP levels in synovial tissues are positively related to OA severity. The ATP levels of the normal group were used as control and set to be 100%. Data are shown as means ± SD. ($n = 5$). The significant differences are determined by the unpaired *t*-test (double tail), $^{***}p < 0.001$, in comparison with the normal group. I) Schematic of mitochondrial dysfunction degree positively associated with OA severity.

of M1 synovial macrophages and therefore the pathogenesis of OA. OA mice models were developed using CIOA and surgical destabilization of the medial meniscus (DMM) in this study. SRA overexpression was used as a measure of M1 macrophage activation.[46] SRA markedly increased in synovial macrophages (F4/80 positive) on day 3 after collagenase injection or day 7 after DMM surgery, and continued to increase on day 28 (Figure S5, Supporting Information), corresponding to early-stage and late-stage OA, respectively. SRA overexpression was also accompanied by elevated expression of IL-1β, TNF-α, and MMP-3 in cartilage and synovium (Figures S6 and S7, Supporting Information). Notably, the number of M1-like macrophages marked by iNOS increased on day 3 post-CIOA and day 7 after DMM surgery (Figure S8, Supporting Information), implying an imbalance of the M1/M2 ratio in OA mice.

The semi-quantitative relationship between OA severity and mitochondrial dysfunction in synovial macrophages was investigated in different stages of OA patients and CIOA mice. We measured the expression of TFAM and mtROS in synovial macrophages, as mtROS can promote mitochondrial damage by suppressing TFAM-mediated mtDNA maintenance. M1 macrophages from human OA synovium exhibited severe mitochondrial damage (Figure 2D), as evidenced by the morphology change, showing the decrease of mitochondrial area to 29% and the length/width ratio to 23.3% (Figure S9, Supporting Information), an 8.2-fold increase in mtROS levels, down to 19.2% in TFAM expression, and down to 55.8% in the ATP level, in comparison with normal human synovium (Figure 2E, Figures S10 and S11, Supporting Information). Meanwhile, M1 macrophages from the early OA synovium in CIOA mice exhibited less mitochondrial damage (Figure 2F), as evidenced by the morphology change, showing the decrease of mitochondrial area to 44.6% and the length/width ratio to 39.6% (Figure S12, Supporting Information), down to 54.0% in mtROS levels, but a 2.37-fold higher TFAM expression than that in the late CIOA synovium (Figure 2G, Figure S13, Supporting Information), suggesting that mitochondrial dysfunction was also exhibited in early OA. In addition, ATP production was reduced in synovial tissues from CIOA mice at the early stage, generating a 2.1-fold increase compared to the late stage (Figure 2H). These results confirmed a positive correlation between OA severity and mitochondrial dysfunction in M1 synovial macrophages (Figure 2I). This suggests that intervention with mitochondrial metabolism is a promising macrophage reprogramming target to prevent the progression of early OA. According to the severe mitochondrial dysfunction of M1 synovial macrophages from both OA patients and CIOA mice models, the biomaterials-based strategy for targeting the mitochondrial metabolism of M1 synovial macrophages holds excellent potential for OA treatment in the clinic.

2.2. Preparation of the Dual-Targeting Meta-Defensome

The positive correlation between OA severity and mitochondrial dysfunction in M1 synovial macrophages was confirmed in both OA patients and mouse models, therefore, we developed a camouflaged meta-Defensome to interfere with the mitochondrial metabolism of M1 macrophages to prevent the progression of early OA. Selective targeting of M1 synovial macrophages was the first requirement for these camouflaged meta-Defensomes to defend mitochondria against metabolic dysfunction. Given the chronic inflammation-directed chemotactic ability of macrophage membrane-coated nanocarriers, it remains unclear whether they can regulate macrophage heterogeneity. To target M1 macrophages and reprogram mitochondria dysfunction, we collected the macrophage membrane and inserted dual-ligands (**Figure 3**A). First, an azide group was introduced onto the surface of macrophages after their incubation with Ac4ManNAz, followed by functionalization with DS through biorthogonal copper-free click chemistry (Figures S14 and S15, Supporting Information). Thereafter, DS served as the targeting moiety for SRA, which is abundant in M1 macrophages in early OA. Meanwhile, MnO_2 NPs (5 nm) and SMT were encapsulated in PLGA nanoparticles using an emulsion solvent evaporation method (Figure S16, Supporting Information) to relieve mitochondria stress caused by mtROS and mtNOS in M1 macrophages, respectively. The DS-bearing macrophage membrane was then introduced to wrap the PLGA nanoparticles through mechanical extrusion. Last, DSPE-PEG_{2000}-TPP was incorporated onto the surface of macrophages, which conferred mitochondrion-targeting ability. This process resulted in a camouflaged meta-Defensome (also named DS/TPP-MMSP), which could potentially defend mitochondria against metabolic dysfunction in M1 macrophages and thus protect the joint from further OA progression. Then, the structural characterization of the camouflaged meta-Defensomes was carried out. The Meta-Defensomes showed a core–shell morphology in the TEM images (Figure 3B) and a narrow size distribution with an average hydrodynamic diameter of approximately 140 nm as measured by DLS (Figure S17A, Supporting Information). Sphere-like MnO_2 nanoclusters appeared to be encapsulated in the core (Figure 3B), with an average size of approximately 5 nm (Figure S18, Supporting Information). Energy-dispersive spectrometry (EDX) also validated the existence of Mn (in yellow) and O (in red) (Figure 3C), while the UV–vis absorption spectra of the meta-Defensome exhibited a broad absorption band at 300–400 nm, corresponding to MnO_2 (Figure S19, Supporting Information). These results suggested the incorporation of MnO_2 into the meta-Defensomes. In addition, the zeta potential of meta-Defensomes was approximately −20 mV (Figures S17B and S20, Supporting Information), endowing it with excellent solubility and long-term colloidal stability (7 days) in the physiological environment (Figure S21, Supporting Information). Next, we confirmed that the modification of DS and TPP ligands had little effect on the biological functions of the macrophage membrane. The typical surface markers of macrophages, such as F4/80 and CD11b, remained in the meta-Defensome (Figure 3D). In addition, the protein composition of the meta-Defensome was consistent with that of the MMSP and the macrophage membrane as shown by gel electrophoresis (Figure S22, Supporting Information). The grafting ratio of DS and TPP on meta-Defensome was determined using high-sensitivity flow cytometry (HSFCM). Rhodamine modified DBCO or DSPE-PEG_{2000}-FITC was inserted into the macrophage membrane following the process of meta-Defensome fabrication, which yielded Rhodamine/FITC-MMSP. Given the concentration of Rhodamine/FITC-MMSP to be 1.99×10^8 particles mL^{-1},

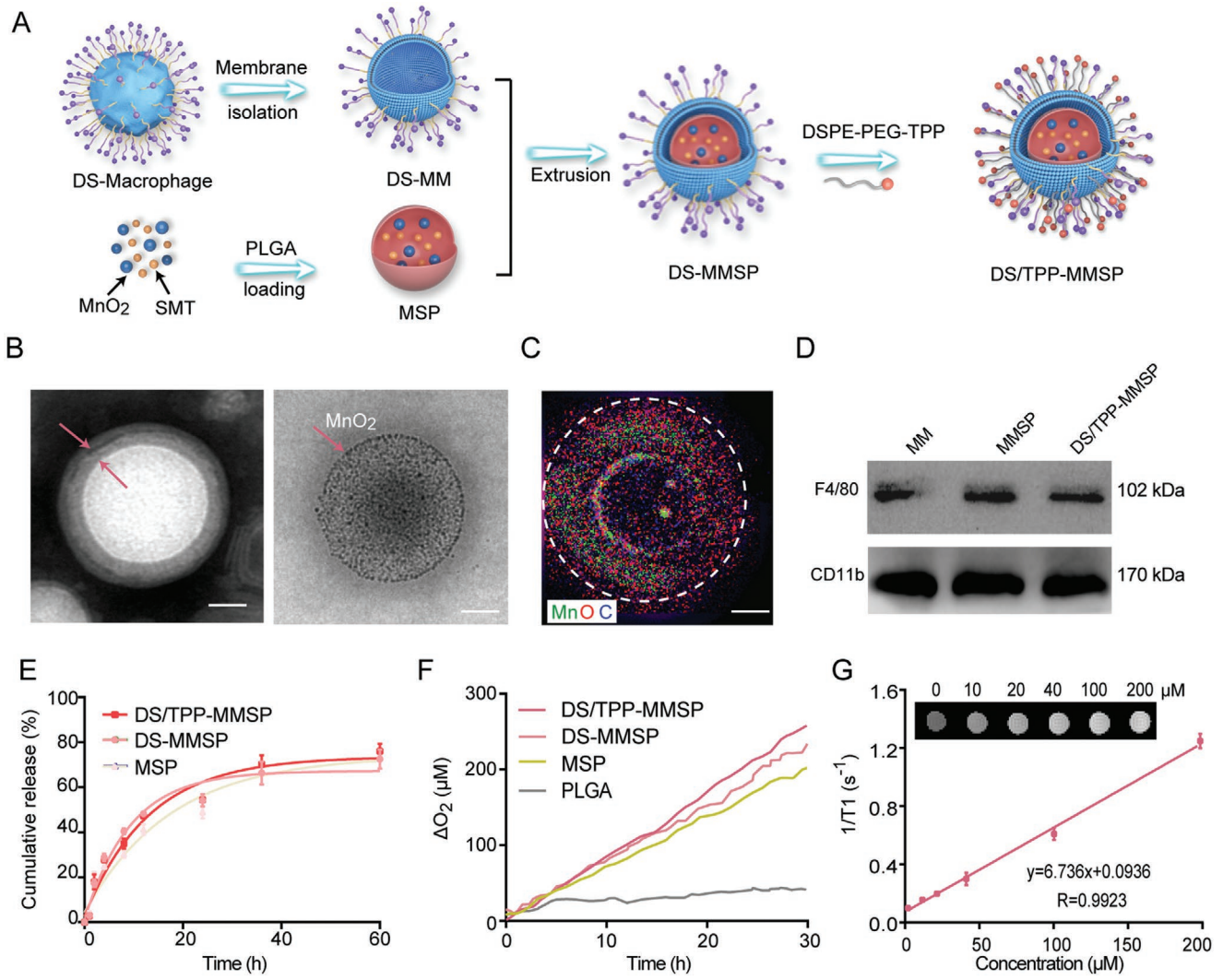

Figure 3. Preparations and Characterization of meta-Defensome. A) Schematics illustrating the preparation of meta-Defensome (DS/TPP-MMSP). B) TEM images of meta-Defensomes. The left column shows the meta-Defensomes stained with phosphotungstic acid, and the arrow indicates the DS-MM on the surface. The right column shows meta-Defensomes without staining, and the arrow indicates MnO_2 nanoparticles. Scale bar: 20 nm. C) EDX mapping of Mn, O, and C elements in meta-Defensomes. Scale bar: 20 nm. D) Western blots of the expression of F4/80 and CD11d of protein sample from meta-Defensomes. E) The line plot shows the release of SMT from meta-Defensomes in PBS within 60 h. Data are shown as means ± SD. ($n = 5$). F) Oxygen production by meta-Defensomes in H_2O_2 within 30 h. G) The r1 characterization of meta-Defensomes. The inset shows T1 images of meta-Defensomes at various concentrations. The linear relationship between signal intensity and meta-Defensomes concentration implied its potential as an imaging agent. Data are shown as means ± SD. ($n = 3$).

we calculated that each meta-Defensome contained an average of ≈680 rhodamine-DS and 487 FITC-TPP, according to the concentration and molecular weight of rhodamine or FITC. Subsequently, the SMT release kinetics of the meta-Defensome were analyzed in a physiological environment. The meta-Defensome (DS/TPP-MMSP) and MMSP exhibited sustained release with no initial burst (Figure 3E). The similar release patterns of meta-Defensome (DS/TPP-MMSP) and MMSP suggested that the ligand modifications had minimal influence on the release kinetics. In addition, the catalytic performance of meta-Defensome enabled by MnO_2 was measured using H_2O_2. A rapid increase in O_2 production was detected upon the addition of meta-Defensome (DS/TPP-MMSP), DS-MMSP, or MMSP to the 10 mM H_2O_2 solution, in contrast to the negligible O_2 production after adding bare PLGA nanoparticles (Figure 3F). Meanwhile, the retention of MR capability of MnO_2 upon encapsulation was confirmed. The T1-weighted signal intensity of the meta-Defensome was positively correlated with the MnO_2 concentration (Figure 3G) with r1 of 6.7 mM^{-1} s^{-1}, close to that of free MnO_2 (6.6 mM^{-1} s^{-1}; Figure S23, Supporting Information).

M1 macrophages-mitochondrial targeting is a prerequisite for an effective therapeutic agent for reprogramming mitochondrial metabolism in M1 macrophages. The selectivity of DS modified macrophage membrane coated PLGA NPs (DS-MP) for M1 macrophages was evaluated using flow cytometry. As shown in Figure S24, Supporting Information, strong green fluorescence was detected in the RAW 246.7-differentiated M1

macrophages after being incubated with C6-loaded DS-MM (DS-MM-C6) for 4 h. In contrast, nearly no fluorescence was observed in mouse fibroblast-like synoviocytes (FLS), MC3T3E1 osteoblasts, ATDC5 chondrocytes, M0 macrophages, and BV2 microglia cells. These results suggest that DS-MM has a good targeting ability for M1 macrophage in the synovial tissue. In addition, the mitochondrial targeting ability of meta-Defensome was also investigated by using co-localization analysis of fluorescence microscopy images. The DS-modified formulations (both DS-MP-C6 and DS/TPP-MP-C6) were almost internalized into the cytoplasm of RAW 246.7-differentiated M1 macrophages (**Figure 4**A,B, Figure S25, Supporting Information), but the unmodified formulation remained outside (MP-C6). As shown in Figure 4B, compared with the unmodified formulation (MP-C6 and TPP-MP-C6), the DS-modified formulation (DS-MP-C6 and DS/TPP-MP-C6) was primarily internalized into the cytoplasm of M1 macrophages (Figure 4B, Figure S25, Supporting Information), indicating that DS modification enhanced cellular accumulation of drugs in activated macrophages. Furthermore, the mitochondrion-targeting capability of the formulations with additional TPP-modification was examined. DS/TPP-MP-C6 (green channel) colocalized with the mitochondrial network (red channel) with a colocalization coefficient R of 0.62 (Figure 4C), which was much higher than that of DS-MP-C6 (R = 0.16). This indicated that DS/TPP-MP had an excellent mitochondrion-targeting capability. It is noteworthy that the total cellular accumulation in M1 macrophages was down to 32% of DS/TPP-MP-C6, although TPP-MP-C6 had a high colocalization coefficient in mitochondria compared to the TPP unmodified formulation (DS-MP-C6 and MP-C6). It suggests that a lack of DS declaration reduced the targeting efficiency of TPP to mitochondria. Therefore, DS/TPP-MP-C6 has a high mitochondria-targeting efficiency in M1 macrophages.

2.3. Oxidative and Energy Metabolism Regulated by Meta-Defensome

The meta-Defensomes containing MnO_2 are supposed to consume excessive mtROS and reduce oxidative stress in M1 macrophages. The ROS-scavenging ability of the meta-Defensomes was evaluated using a MitoSOX fluorescent probe and we found a significant reduction in mtROS levels of M1 macrophages compared to the control groups (Figure 4D). Moreover, meta-Defensomes exhibited an effective ROS scavenging capability (Figure S26, Supporting Information), which was down to 17.8% in ROS levels than that in M1 macrophages. Meta-Defensomes upregulated the expression of mtNOS in the dysfunctional mitochondria of M1 macrophages (Figure S27, Supporting Information), thereby significantly reducing NO production in M1 macrophages (Figure S28, Supporting Information). Taken together, MnO_2- and SMT-encapsulated meta-Defensomes are capable of regulating oxidative metabolism by scavenging mtROS and increasing mtNOS activity.

The regulation of intracellular energy metabolism by the meta-Defensomes was further evaluated using an ATP assay in M1 macrophages. The results showed that meta-Defensomes promoted ATP production (Figure 4E) and markedly increased mitochondrial succinate dehydrogenase activity (Figure S29, Supporting Information). At the same time, these particles inhibited glycolytic capacity and promoted aerobic glycolysis of M1 macrophages, as evidenced by the increased OCR level and decreased ECAR levels (Figure 4F, Figure S30, Supporting Information). In addition, the increased expression of HIF-1α by stimulation with LPS plus IFN-γ, which could activate glycolysis metabolism and inhibit mitochondrial oxidation in macrophages,[47] was also suppressed by meta-Defensomes in M1 macrophages. In short, this suggests that meta-Defensomes are potent in promoting energy generation and reprogramming the metabolic pathway of M1 macrophages.

2.4. M1 Macrophage Repolarization by Meta-Defensome

Given the excellent ability of meta-Defensomes to regulate intracellular oxidative metabolism and energy metabolism in M1 macrophages, we examined the polarization of RAW264.7 cells-differentiated macrophages. A notable decrease in iNOS and an increase in CD206 were observed in M1-polarized RAW264.7 after meta-Defensomes treatment (Figure 4G, Figure S31, Supporting Information). After incubation with meta-Defensomes, the number of $F4/80^+iNOS^+$ cells (M1 macrophage) was decreased from 56.3% to 9.68%, indicating that meta-Defensomes repolarized M1 macrophages with a high efficiency of 82.8%. Meanwhile, the number of $F4/80^+CD206^+$ cells (M2 macrophage) was increased from 4.22% to 42.6%, suggesting that meta-Defensomes transformed M1 macrophages into M2 phenotype with a high efficiency of 82.3%. In comparison with DS modified macrophage nanocarriers, the transformation efficiency from M1 macrophage into M2 of DS-MMSP is down to 65.0% of meta-Defensomes group, demonstrating that the regulation of mitochondria metabolism processed of excellent M1 macrophage transformation ability. A consistent transformation trend was confirmed using immunofluorescence staining for iNOS and CD206. It was observed that M1-polarized RAW264.7 cells (iNOS-positive) were almost totally transformed into M2-polarized RAW264.7 cells (CD206-positive; Figure 4H). In contrast, meta-Defensomes appeared to protect M2-polarized RAW264.7 cells from being pathologically transformed into M1 macrophage polarization. Despite stimulating M2-polarized RAW264.7 cells with LPS plus IFN-γ that mimics the synovitis microenvironment, a negligible M1 marker (iNOS) appeared but high level of M2 marker (CD206, green) remained (Figures S32 and S33, Supporting Information). These results demonstrated that meta-Defensomes effectively induced the repolarization of M1 macrophages and protected M2 macrophages from being transformed into the M1 phenotype.

2.5. Mitochondrial Function Recovery by Meta-Defensome via TFAM Upregulation

To investigate the underlying mechanism of mitochondrial metabolic reprogramming in M1 macrophages by meta-Defensomes, the expression of COXIV, ATP5A and TOMM20 was examined, considering their essential roles in mitochondrial function. COX IV is one of the subunits of the cytochrome

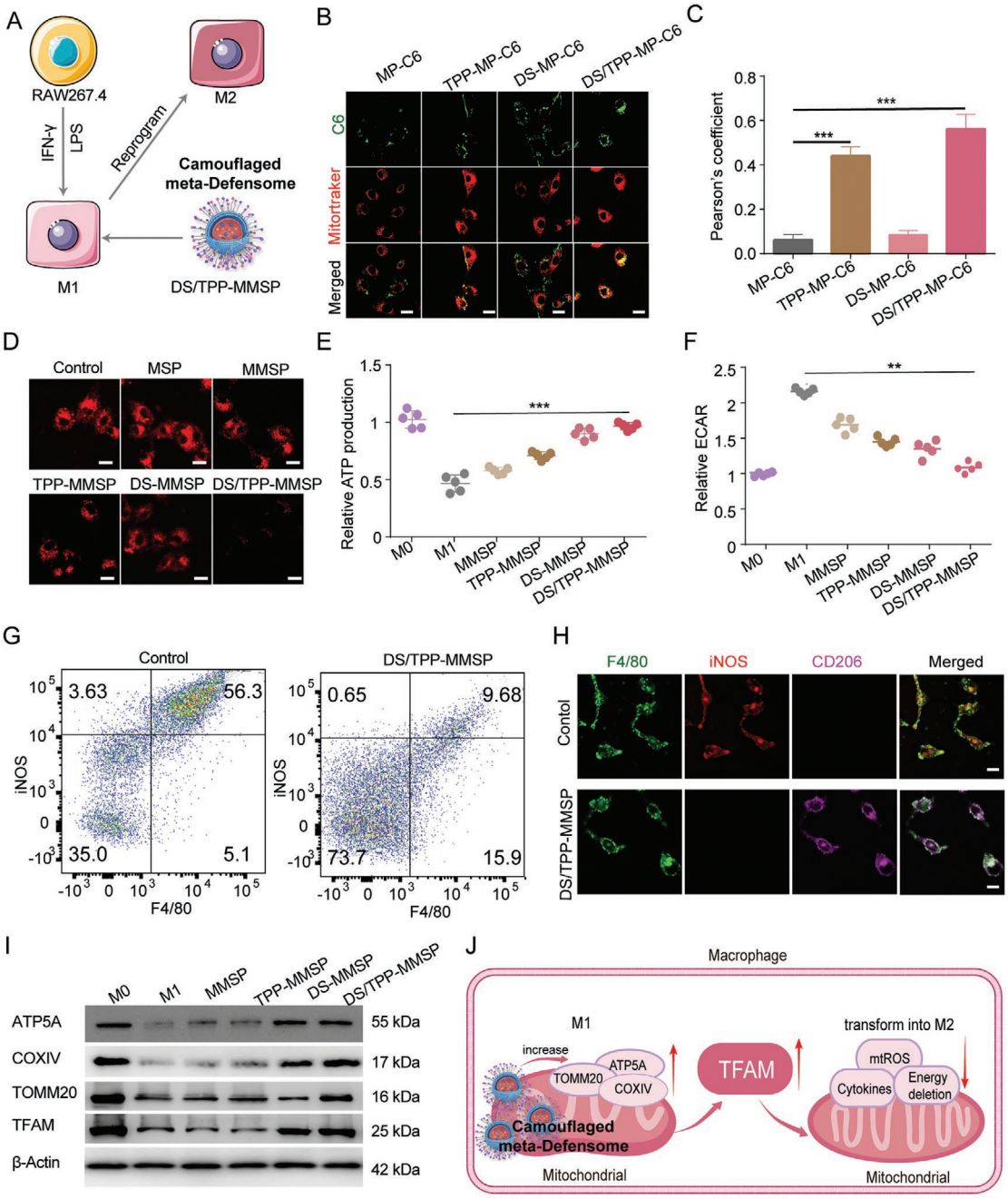

Figure 4. The reprogramming of M1 macrophage polarization by meta-Defensome. A) Schematics illustrating the reprogramming of M1 macrophages into M2 macrophages by meta-Defensome (DS/TPP-MMSP) treatment. B) Confocal laser scanning imaging showing the colocalization of C6-labeled multi-stage formulations in mitochondria of differentiated M1 macrophages. C6 (green) and Mitortracker for mitochondria staining (red) were observed. Scale bar: 20 µm. C) Colocalization coefficient of C6-labeled multi-stage formulations with mitochondria in M1 macrophages. Data are shown as means ± SD. ($n = 5$). The significant differences are determined by the unpaired t-test (double tail), $^{***}p < 0.001$, in comparison with the control group (MP-C6). D) Confocal laser scanning imaging shows the decreased mtROS in M1 macrophages upon meta-Defensomes treatment. Scale bar: 20 µm. E) Bar chart of relative ATP production in M1 macrophages upon meta-Defensomes treatment. The ATP production of the M0 macrophage group was used as control and set to be 1. Data are shown as means ± SD. ($n = 5$). The significant differences are determined by the unpaired t-test (double tail), $^{***}p < 0.001$, in comparison with the M1 macrophage group. F) Bar chart of relative ECAR level in M1 macrophages upon meta-Defensomes treatment. The ECAR level of the M0 macrophage group was used as control and set to be 1. Data are shown as means ± SD. ($n = 5$). The significant differences are determined by the unpaired t-test (double tail), $^{***}p < 0.001$, in comparison with M1 macrophage group. G) Flow cytometry shows the increased ratio of M1 macrophages upon meta-Defensomes treatment (stained with F4/80 and iNOS). H) Confocal laser scanning imaging of M1 macrophages labeled with F4/80 (green), iNOS (red), and CD206 (purple) before and after treatment with meta-Defensomes. Scale bar: 20 µm. I) Western blots show the expression of COX IV, ATP5A, TOMM20, and TFAM in M1 macrophages upon different treatments. J) Schematic illustrates that mitochondrial dysfunction in M1 macrophage was reversed by inhibiting TFAM deficiency upon meta-Defensomes treatment.

C Oxidase (COX) hetero-oligomeric enzyme located in the inner mitochondrial membrane, which drives ATP synthesis by catalyzing molecular oxygen into water and translocating protons across the inner mitochondria membrane.[48] ATP5A is a catalytic subunit of the mitochondrial ATP synthase complex responsible for the synthesis and hydrolysis of ATP.[49] The expression of COX IV and ATP 5A was upregulated after meta-Defensomes treatment, in contrast to macrophages treated with MMSP (Figure 4I), indicating meta-Defensomes can regulate the ATP supply in M1 macrophages. The mitochondrial electron transport chain utilizes a series of electron transfer reactions to generate cellular ATP through oxidative phosphorylation (OXPHOS).[50] Mitochondrial OXPHOS is inhibited in activated M1 macrophages, rendering them unable to be converted into M2 phenotype.[51] As shown in Figure S34A, Supporting Information, the expression level of ATP5A, UQCRC2, and SDHB were increased in M1 macrophages after meta-Defensomes treatments. However, the expression levels of OXPHOS system remained unchanged in M2 macrophages after co-cultured with meta-Defensomes (Figure S34B, Supporting Information). These results indicated that meta-Defensomes can regulate OXPHOS in M1 macrophages to restore mitochondria ATP supply while do not affect the disturb the electron transport chain during oxidative phosphorylation in M2 macrophages. Meanwhile, meta-Defensomes promoted mitochondrial biogenesis, as shown by the upregulation of TOMM20 (a marker of mitochondrial content; Figure 4I).[52]

In addition, the protein levels of TFAM in M1 were lower than in M2.[53] Meta-Defensomes were found to restore TFAM expression, which might subsequently restore mitochondrial metabolism in M1 macrophages. Furthermore, meta-Defensomes were found to inhibit the secretion of inflammatory factors in M1 macrophages (Figures S35 and S36, Supporting Information), including TNF-α and IL-1β, which were 3.1-fold and 2.3-fold lower than those in the TPP-MMSP groups, respectively. Furthermore, meta-Defensomes induced negligible apoptosis in chondrocytes (Figure S37, Supporting Information), indicating good cellular biocompatibility. Additionally, the supernatant of M1 macrophages cultured with meta-Defensomes significantly inhibited MMP-13 protein expression in ATDC5 cells (Figure S38, Supporting Information). These results suggest that meta-Defensomes may protect chondrocytes from the inflammatory microenvironment in OA joints. In summary, our work demonstrated that meta-Defensomes could repolarize M1 macrophages by reversing mitochondrial dysfunction in a TFAM-dependent manner (Figure 4J).

2.6. Alleviating the Progression of Disease in CIOA Mice

Macrophage membrane-coated nanocarriers exhibit high targeting efficiencies in various inflammatory diseases.[32] In addition, no obvious immunotoxicity was observed in mice administered with external macrophages, even at the highest dosage (10^9 macrophages kg^{-1}),[54] indicating the good biocompatibility of macrophage membrane-coated nanocarriers in vivo. In this study, mouse peritoneal macrophages were selected as live cell-based carriers for camouflaged defense mechanisms. To systemically evaluate the biocompatibility of DS- and TPP- modified macrophage membrane-coated PLGA NPs (DS/TPP-MP), three groups of C57BL/6 mice were i.v. injected with saline, macrophage membrane-coated PLGA NPs (MP), and DS/TPP-MP for half a month with a high dose of 10 mg kg^{-1} every four days (for four injections). The body weight (Figure S39A, Supporting Information) and counts of immune-associated cells including monocytes, lymphocytes, and neutrophils, in the blood (Figure S39B, Supporting Information) of the treated mice were similar to those in the control group. In addition, histological analysis of the main organs (including the liver, lungs, kidneys, and spleen) of mice treated with DS/TPP-MP indicated no toxicity (Figure S39C, Supporting Information). Furthermore, the liver function biomarkers alanine transaminase (ALT) (Figure S39D, Supporting Information) and aspartate aminotransferase (AST) (Figure S39E, Supporting Information) and kidney function biomarkers blood urea nitrogen (BUN) (Figure S39F, Supporting Information) in the serum of mice treated with DS/TPP-MP were comparable to those of the saline-treated group. These results demonstrated that no obvious immunotoxicity occurred in mice administered macrophage membrane-coated nanocarriers, even at the highest dosage.

To determine the synovium-targeting ability of the camouflaged meta-Defensome, DiR-labeled DS/TPP-MMP was intravenously injected into the tail vein of early-stage CIOA mice. The accumulation of DS/TPP-MMP in the knee joint was quantified using an IVIS imaging system. Robust fluorescence (DiR) was observed shortly in OA knees at 4 h post-injection of DS/TPP-MMP, and continued to increase within 12 h post-injection, reaching a 1.9-fold higher level than the DS-MMP group (**Figure 5**A,B). This implies their excellent targeting ability for OA joints and their long-period retention. In addition, ex vivo imaging showed fluorescence in the inflamed joints of CIOA mice after treatment with DiR-DS/TPP-MMP and DiR-DS-MMP compared to DiR-MMP, indicating that DS modification can improve the targeting ability of macrophage membrane-coated nanocarriers. Furthermore, more DiR-DS/TPP-MMP accumulated in OA joints than DiR-DS-MMP, suggesting that the dual ligand (DS and TPP) targeting strategy has OA good targeting ability in vivo. Importantly, a lower distribution of DiR signals in the liver and spleen was observed in the DiR-DS/TPP-MMP group than in the DiR-MMP and DiR-DS-MMP groups, confirming that DS/TPP-MMP has high selectivity toward OA inflammatory joints (Figure S40, Supporting Information). Notably, further investigations revealed that DS/TPP-MMP was specifically enriched in the articular synovium of CIOA mice, in contrast to MMP (Figure S41, Supporting Information). DS/TPP-MMP also allowed in vivo MRI of synovial macrophages, once intravenously injected into OA mice (Figure 5C), consistent with the results shown in Figure 3G. The T1 signal appeared stronger in knees of CIOA mice at 12 h-post-injection than in MMP-treated CIOA mice, in agreement with the trend in IVIS imaging (Figure 5A). These results confirmed the synovium targeting of meta-Defensomes in the early stages of OA.

Subsequently, we investigated whether meta-Defensomes effectively suppressed OA progression in vivo through intravenous injection (Figure 5D). Compared with the saline control, meta-Defensomes effectively reduced the levels of inflammatory

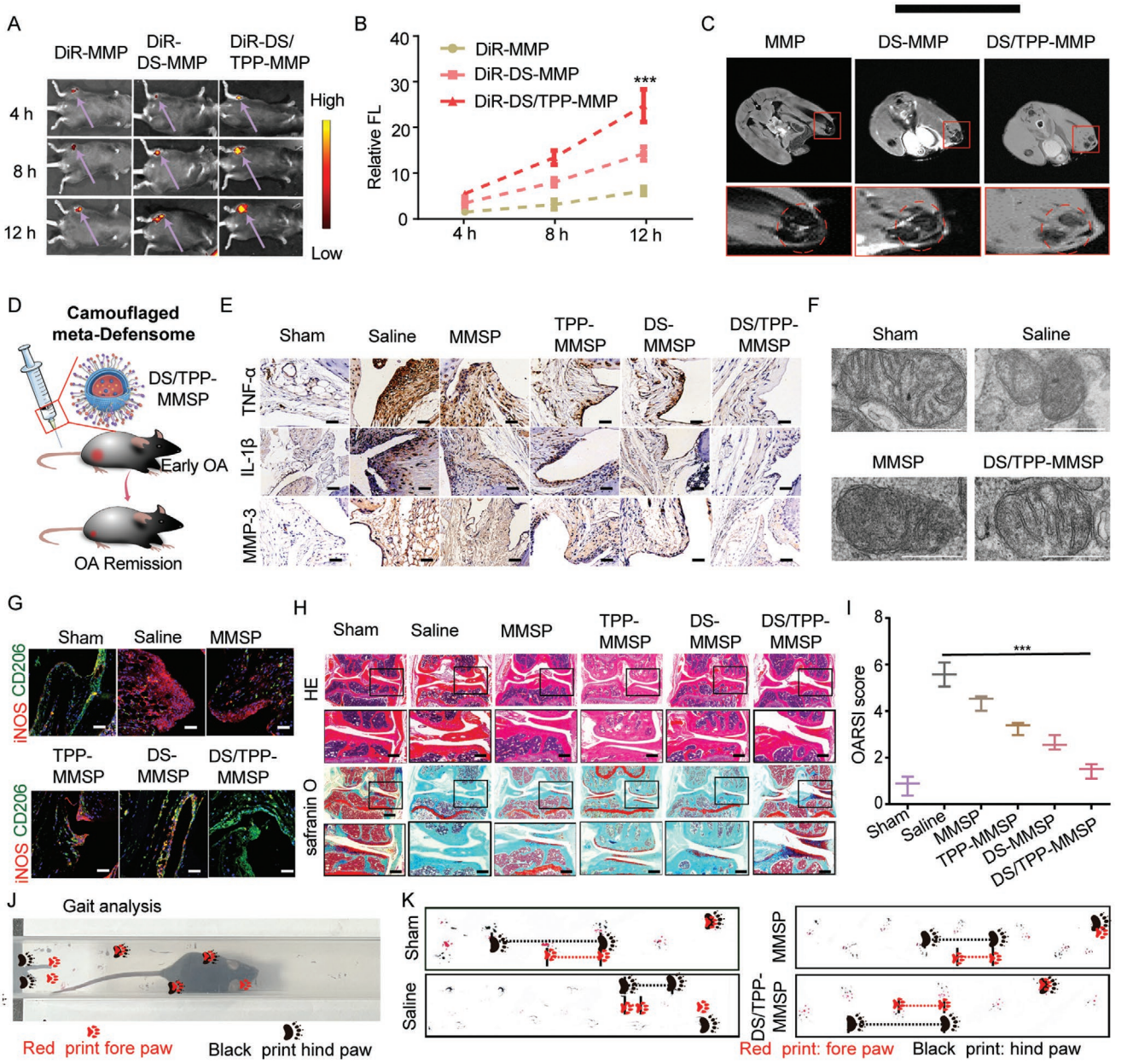

Figure 5. Meta-Defensome attenuated OA by inducing synovial macrophage M1 repolarization. A) In vivo imaging of CIOA mice after 4, 8, and 12-h treatment of DiR-labeled DS/TPP-MMP (meta-Defensome). B) Bar chart of relative fluorescence intensity (FL) of knee joints in (A). The fluorescence intensity of paw tissue was used as control and set to be 1. Data are shown as means ± SD. ($n = 3$). The significant differences are determined by the unpaired t-test (double tail), $^{***}p < 0.001$, in comparison with the DiR-MMP group. C) T1 images of CIOA mice after treatment of MMP, DS-MMP, and DS/TPP-MMP. The circle indicates knee joints. The T1 signal of knee joints from CIOA mice after treatment with DS/TPP-MMP was much higher than that of other groups. D) Schematics illustrating meta-Defensomes treatment attenuates OA in model mice. E) Representative immunohistochemistry images of TNF-α, IL-1β, and MMP3 in the synovium from CIOA mice upon corresponding treatments. Scale bar: 100 µm. F) TEM images of the mitochondria of synovial macrophage from CIOA mice treated with different treatments. Scale bars: 500 nm. G) Immunofluorescence of iNOS and CD206 in the synovium from CIOA mice treated with different treatments. Scale bars: 50 µm. H) H&E and safranin O staining of the joint from CIOA mice after meta-Defensomes treatment. Scale bar: 50 µm. I) The severity of OA-like phenotype was analyzed by grading histological sections in medial femoral condyles (MFCs) and the medial tibial plateau (MTP) using the OARSI score system. The OARSI score of sham group was used as control and set to be 1. Data are shown as means ± SD. ($n = 6$). The significant differences are determined by the unpaired t-test (double tail), $^{***}p < 0.001$, in a comparison with saline group. J) Schematics illustrating gait analysis for OA mice. K) Gait analysis for CIOA mice treated with meta-Defensomes treatment. The red dotted line represents stride length; the black dotted line represents step length. Red print: fore paw; black print: hind paw.

factors (TNF-α and IL-1β) and matrix metallopeptidase 3 (MMP3). More importantly, the expression of inflammatory factors in early OA mice treated with meta-Defensomes seemed negligible compared to that in sham groups, indicating that meta-Defensomes can effectively alleviate synovitis in OA (Figure 5E). Importantly, the mitochondrial morphology

recovered, showing less swelling but more organized mitochondrial cristae, mitochondrial area, and mitochondrial length to width after meta-Defensomes treatment, compared to the other groups (Figure 5F, Figure S42, Supporting Information). In addition, a greater number of CD206-positive cells were observed in the synovium of CIOA mice treated with meta-Defensomes than in those treated with saline (Figure 5G), suggesting that successful inhibition of M1 polarization of synovial macrophages in CIOA mice. Meanwhile, TFAM expression in iNOS-positive M1 macrophages was also significantly restored by meta-Defensomes compared to other groups, which indicated that the recovery of mitochondrial dysfunction in synovial tissues was beneficial to facilitating M1 macrophage repolarization (Figure S43, Supporting Information). To further confirm that meta-Defensomes could relieve joint inflammation and reduce cartilage destruction, joints of CIOA mice were sectioned for histological analysis at the study endpoint (4 weeks after meta-Defensomes treatments). Prominent synovial hyperplasia was observed in the joints of mice intra-articularly injected with collagenase and was significantly inhibited by treatment with meta-Defensomes (Figure 5H, upper row). Meanwhile, reduced safranin O staining of proteoglycans and exacerbated cartilage surface erosion was observed in CIOA mice injected with saline. In contrast, the intravenous injection of meta-Defensomes ameliorated OA pathology (Figure 5H, lower row). In addition, severe cartilage erosion can occur in CIOA mice. The administration of meta-Defensomes caused a remarkable (though not full) reduction in cartilage degradation, as evident from the Osteoarthritis Research Society International (OARSI) scores (Figure 5H,I).

Additionally, we evaluated the biosafety of the meta-Defensomes in vivo. H&E staining of organs in mice revealed no histopathological abnormalities or lesions after meta-Defensomes injection compared with those in the saline group (Figure S44, Supporting Information). Meanwhile, routine blood testing showed few differences between the meta-Defensomes and control groups, suggesting that meta-Defensomes might have little negative influence on the circulatory system (Figure S45, Supporting Information). Collectively, these results suggest that meta-Defensomes have good biosafety and could be used as a promising therapeutic drug for OA treatment.

Finally, we performed gait analysis to assess pain management in CIOA. The separation of the prints of the hind and forepaws on the affected side and the changes in step length and stride length were used to reflect the claudication of the mice during walking (Figure 5J). As shown in Figure 5K, after meta-Defensomes treatment, the prints of the front and hind paws relatively overlapped, and the step length and stride length were more similar to those of the sham group compared to other groups, indicating that claudication was greatly relieved by meta-Defensomes treatment. This excellent therapeutic effect on early OA mice might be ascribed to the effective reprogramming of mitochondria metabolism and therefore the repolarization of M1 macrophages into the M2 phenotype.

3. Conclusion

This study establishes a camouflaged meta-Defensome that specifically targets activated macrophages via receptor-ligand interactions and selectively accumulates in mitochondria through electrostatic attraction between TPP and mitochondria. More importantly, meta-Defensomes targeted synovitis in early-stage OA joints in response to inflammation and effectively recognized M1 macrophages by targeting the SRA receptor, thereby allowing real-time visualization of synovial macrophages through bimodal (MRI/IVIS) imaging. In vitro studies showed that the mitochondrial metabolism of M1 synovial macrophages was reprogrammed by scavenging mtROS while inhibiting mtNOS, which restored aerobic respiration by increasing TFAM expression, thereby effectively repolarizing the M2 phenotype. The meta-Defensomes effectively defended the OA synovium against inflammatory stress and protected cartilage from degeneration. This clearly shows that reprogramming mitochondrial metabolism can be a promising strategy to delay OA progression and that the newly developed meta-Defensome holds great potential for OA treatment in clinical practice.

4. Experimental Section

Patient Samples: The human synovium samples were collected from three patients with OA patients undergoing joint replacement surgery. The normal synovium samples were obtained from three patients with no synovitis and no cartilage injury, as confirmed by arthroscopic examination. All samples were collected from Drum Tower Hospital Affiliated to the Medical School of Nanjing University. Informed consent was obtained from all patients, and ethical approval was obtained from the Ethics Committee of Drum Tower Hospital Affiliated to the Medical School of Nanjing University (approval No. 2020-156-01).

Modification of DS on the Surface of Macrophages: Fresh mouse peritoneal macrophages from C57BL/6 mice were harvested according to previously reported method.[55] The mice were intraperitoneally injected with 1 mL 4% thioglycolate broth for 3 days before being sacrificed and disinfected by immersing in 75% ethanol. The body was then injected with 5 mL Dulbecco's modified Eagle medium (DMEM) in enterocoelia followed by a full massage. The withdrawn DMEM containing fresh peritoneal macrophage was collected and cultured in DMEM containing 10% FBS maintained in CO_2 incubator. Since sialic acids presented on the macrophage surface,[56] the macrophages were incubated with Ac4ManNAz (10×10^{-6} M) to generate azide groups on the surface through the sialic acid pathway. After 48 h of incubation, macrophages were washed twice with PBS and treated with serum-free medium containing DBCO-DS (10×10^{-6} M) for 2 h. After washing the cells twice with PBS, the DS modified macrophages membrane (DS-MM) was obtained through freezing and thawing for 3 cycles.

Preparation of PLGA-MnO_2/STM NPs (MSP): MnO_2 NPs were synthesized by reducing potassium permanganate with polyallylamine hydrochloride (PAH).[57] Briefly, KMnO4 (30 mg mL^{-1}) was mixed with PAH (30 mg mL^{-1}). After reacting for 30 min, MnO_2 NPs were obtained after purification. The synthesized MnO_2 NPs and S-methylisothiourea (STM) were encapsulated into PLGA to produce MnO_2/STM-PLGA NPs (MMP) by a modified double-emulsion solvent-evaporation method.[58] Briefly, PLGA (200 mg) was dissolved in 2 mL of ethyl acetate with STM (10 mg) and MnO_2 NPs (10 mg). Poly(vinyl alcohol) (PVA, 5% w/v) was added drop by drop to the previous solution with intermittent vertexing. MSP was obtained after being washed with pure water several times.

Preparation of Meta-Defensomes: DS-MM were sonicated for 6 min using a sonicator, and DS-MA membrane vesicles were obtained by repeatedly extruding through 400 nm, 200 nm, and 100 nm polycarbonate porous membranes using a mini extruder (Avanti Polar Lipids, AL, USA). MSP at 5 mg mL^{-1} was mixed with 1 mL of DS-MA membrane vesicles, followed by extrusion through a 100 nm polycarbonate membrane at least 5 times to obtain DS-MMSP. Finally, DSPE-PEG200-TPP was incubated with DS-MMSP for 4 h at 37 °C in

PBS (pH 7.4), then meta-Defensomes were prepared. These NPs were characterized for size and zeta potential by Dynamic Light Scattering. The TEM images and EDX of DS/TPP MMPs were measured by transmission electron microscopy. The amount of SMT was determined by HPLC methods, and the amount of manganese was evaluated with ICP-MS. SMT or Mn encapsulation capacity was calculated as $EC_{SMT}\% = ((W_{added\text{-}SMT\text{-}or\text{-}Mn} - W_{unencapsulated\text{-}SMT\text{-}or\text{-}Mn})/W_{added\text{-}SMT\text{-}or\text{-}Mn}) \times 100\%$, SMT or Mn loading capacity was calculated as $LC_{SMT}\% = ((W_{added\text{-}SMT\text{-}or\text{-}Mn} - W_{unencapsulated\ SMT\text{-}or\text{-}Mn})/W_{meta\text{-}Defensome\text{-}(DS/TPP\text{-}MMSP)}) \times 100\%$. The encapsulation efficiency of SMT in meta-Defensomes was approximately 45.3%. The drug-loading capacity of SMT or Mn in meta-Defensomes was approximately 4.3% or 8.8%. The encapsulation efficiency of in meta-Defensomes was approximately 25.3% or 35.6%.

Macrophage Polarization Detection: RAW264.7 cells pretreated with LPS plus IFN-γ (24 h) were co-cultured with meta-Defensomes for 24 h (1 mg mL^{-1}). Subsequently, the cells were washed thrice with PBS and fixed with a 4% paraformaldehyde solution. After being incubated with 0.2% Triton X-100 in PBS for 20 min, the cells were blocked with 1% BSA in DPBS for 45 min. Then, the cells were treated with anti-iNOS antibody-PE or anti-CD206 antibody Alexa Fluor 488 at 4 °C for 30 min. Thereafter, fluorescence images of cells were obtained using a confocal laser microscope.

Treatment of CIOA Mice: C57BL/6 mice were purchased from the Model Animal Research Center of Nanjing University. All mice were kept under pathogen-free and 12 h light/dark cycle conditions with sufficient food and water. Animal use and experimental protocols were reviewed and approved by the Animal Care Committee of Nanjing University, in accordance with the guidelines of the Institutional Animal Care and Use Committee (2021AE01031). CIOA was induced by two intra-articular injections of 1 U collagenase type VII into knee joints of 10-week-old male C57BL/6 at the right knee joint on day 0 and day 2, causing damage to collateral and cruciate ligaments leading to joint dysfunction of the knee joint.[36] The sham operation with the control mice of the same age was performed with intra-articular injections of saline. CIOA mice were i.v. injected with meta-Defensomes (100 µL, 1 mg mL^{-1}) every 2 days for 2week. At study endpoints, mice were euthanized, and the joints were collected for H&E staining and safranin O-fast green staining. The safranin O-fast green sections were evaluated utilizing the OARSI score, which scored the product of six grades (depth of lesion) and four stages (extent of involvement) on a scale of 0 (normal) to 24 (severe osteoarthritis).

Statistical Analysis: The data analyzed with normalization are specified in the figure legends. All data were presented as the mean ± standard deviation (SD). For single-cell RNA sequencing analysis for human synovium, $n = 3$; in vivo imaging studies, $n = 3$ mice in each group; the r1 characterization, $n = 3$; quantification of mitochondrial area, $n = 6$; the ratio of mitochondrial length to width, $n = 6$; CIOA mice treatment, $n = 6$ mice in each group; otherwise, $n = 5$. An unpaired two-tailed *t*-test was used to calculate the significance of differences (p value). $p < 0.05$ was considered to demonstrate statistically significant differences. Statistical analysis was performed using SPSS software (version 13.0; Social Inc. IL, Chicago, USA)."

Supporting Information

Supporting Information is available from the Wiley Online Library or from the author.

Acknowledgements

L.Z. and X.C. contributed equally to this work. This work was supported by the Key Program of NSFC (81730067), Major Project of NSFC (81991514), Jiangsu Provincial Key Medical Center Foundation, Jiangsu Provincial Medical Outstanding Talent Foundation, Jiangsu Provincial Medical Youth Talent Foundation and Jiangsu Provincial Key Medical Talent Foundation, the Fundamental Research Funds for the Central Universities (14380493, 14380494), National Science Foundation of China (Grant No 82002370, 31800806, 82000069), China Postdoctoral Science Foundation (Grant No 2019M661806), Natural science foundation of Jiangsu province (Grant No BK20200117, BK20200314), Jiangsu postdoctoral research support project (Grant No 2021K059A), and Program of Innovation and Entrepreneurship of Jiangsu Province.

Conflict of Interest

The authors declare no conflict of interest.

Data Availability Statement

The data that support the findings of this study are available from the corresponding author upon reasonable request.

Keywords

denfensomes, mitochondrial dysfunction, mitochondrial targeting, nanoenzymes, osteoarthritis, synovial macrophages

Received: March 24, 2022
Revised: May 30, 2022
Published online: June 23, 2022

[1] a) T. Kato, S. Miyaki, H. Ishitobi, Y. Nakamura, T. Nakasa, M. K. Lotz, M. Ochi, *Arthritis Res. Ther.* **2014**, *16*, R163; b) B. J. de Lange-Brokaar, A. Ioan-Facsinay, G. J. van Osch, A. M. Zuurmond, J. Schoones, R. E. Toes, T. W. Huizinga, M. Kloppenburg, *Osteoarthritis Cartilage* **2012**, *20*, 1484; c) M. J. Benito, D. J. Veale, O. FitzGerald, W. B. van den Berg, B. Bresnihan, *Ann. Rheum. Dis.* **2005**, *64*, 1263; d) A. Kennedy, U. Fearon, D. J. Veale, C. Godson, *Front. Immunol.* **2011**, *2*, 52; e) X. Fan, X. Wu, L. Trevisan Franca De Lima, S. Stehbens, C. Punyadeera, R. Webb, B. Hamilton, V. Ayyapann, C. McLauchlan, R. Crawford, M. Zheng, Y. Xiao, I. Prasadam, *FASEB J.* **2022**, *36*, e22142; f) Y. Wang, D. Yu, Z. Liu, F. Zhou, J. Dai, B. Wu, J. Zhou, B. C. Heng, X. H. Zou, H. Ouyang, H. Liu, *Stem Cell Res. Ther.* **2017**, *8*, 189; g) X. Zhu, F. Chen, K. Lu, A. Wei, Q. Jiang, W. Cao, *Ann. Rheum. Dis.* **2019**, *78*, 1420.

[2] a) K. Lu, T. S. Shi, S. Y. Shen, Y. Shi, H. L. Gao, J. Wu, X. Lu, X. Gao, H. X. Ju, W. Wang, Y. Cao, D. Chen, C. J. Li, B. Xue, Q. Jiang, *Cell Metab.* **2022**, *34*, 441; b) X. Chen, X. Zhu, A. Wei, F. Chen, Q. Gao, K. Lu, Q. Jiang, W. Cao, *Bone Res.* **2021**, *9*, 15; c) X. Chen, W. Gong, X. Shao, T. Shi, L. Zhang, J. Dong, Y. Shi, S. Shen, J. Qin, Q. Jiang, B. Guo, *Ann. Rheum. Dis.* **2022**, *81*, 85; d) W. Lin, J. Klein, *Adv. Mater.* **2021**, *33*, 2005513; e) J. Collison, *Nat. Rev. Rheumatol.* **2019**, *15*, 573.

[3] a) T. Wang, A. Wagner, R. Gehwolf, W. Yan, F. S. Passini, C. Thien, N. Weissenbacher, Z. Lin, C. Lehner, H. Teng, C. Wittner, Q. Zheng, J. Dai, M. Ni, A. Wang, J. Papadimitriou, T. Leys, R. S. Tuan, S. Senck, J. G. Snedeker, H. Tempfer, Q. Jiang, M. H. Zheng, A. Traweger, *Sci. Transl. Med.* **2021**, *13*, eabe5738; b) D. J. Hunter, D. Schofield, E. Callander, *Nat. Rev. Rheumatol.* **2014**, *10*, 437; c) E. M. Roos, N. K. Arden, *Nat. Rev. Rheumatol.* **2016**, *12*, 92; d) S. M. Bierma-Zeinstra, B. W. Koes, *Nat. Clin. Pract. Rheumatol.* **2007**, *3*, 78.

[4] a) M. Rahmati, A. Mobasheri, M. Mozafari, *Bone* **2016**, *85*, 81; b) E. W. Orlowsky, V. B. Kraus, *J. Rheumatol.* **2015**, *42*, 363.

[5] a) S. Brown, S. Kumar, B. Sharma, *Acta Biomater.* **2019**, *93*, 239; b) M. Gharagozloo, S. Majewski, M. Foldvari, *Nanomedicine* **2015**,

11, 1003; c) S. B. Abramson, M. Attur, Y. Yazici, *Nat. Clin. Pract. Rheumatol.* **2006**, *2*, 304; d) M. Englund, F. W. Roemer, D. Hayashi, M. D. Crema, A. Guermazi, *Nat. Rev. Rheumatol.* **2012**, *8*, 412.

[6] a) H. Kamaruzaman, P. Kinghorn, R. Oppong, *BMC Musculoskeletal Disord.* **2017**, *18*, 183; b) P. G. Conaghan, M. A. D'Agostino, M. Le Bars, G. Baron, N. Schmidely, R. Wakefield, P. Ravaud, W. Grassi, E. Martin-Mola, A. So, M. Backhaus, M. Malaise, P. Emery, M. Dougados, *Ann. Rheum. Dis.* **2010**, *69*, 644.

[7] a) A. Mathiessen, P. G. Conaghan, *Arthritis Res. Ther.* **2017**, *19*, 18; b) A. J. Smith, P. Dieppe, K. Vernon, M. Porter, A. W. Blom, *Lancet* **2012**, *379*, 1199.

[8] a) H. Zhang, D. Cai, X. Bai, *Osteoarthritis Cartilage* **2020**, *28*, 555; b) L. E. Miller, H.-p. Jüsten, J. Schcölmerich, R. H. Straub, *FASEB J.* **2000**, *14*, 2097.

[9] S. Tardito, G. Martinelli, S. Soldano, S. Paolino, G. Pacini, M. Patane, E. Alessandri, V. Smith, M. Cutolo, *Autoimmun. Rev.* **2019**, *18*, 102397.

[10] a) F. Wang, S. Zhang, R. Jeon, I. Vuckovic, X. Jiang, A. Lerman, C. D. Folmes, P. D. Dzeja, J. Herrmann, *EBioMedicine* **2018**, *30*, 303; b) F. Zhou, J. Mei, X. Han, H. Li, S. Yang, M. Wang, L. Chu, H. Qiao, T. Tang, *Acta Pharm. Sin. B* **2019**, *9*, 973.

[11] a) A. Covarrubias, V. Byles, T. Horng, *Cell Res.* **2013**, *23*, 984; b) E. M. Palmieri, M. Gonzalez-Cotto, W. A. Baseler, L. C. Davies, B. Ghesquière, N. Maio, C. M. Rice, T. A. Rouault, T. Cassel, R. M. Higashi, A. N. Lane, T. W. Fan, D. A. Wink, D. W. McVicar, *Nat. Commun.* **2020**, *11*, 698; c) M. Wang, M. Chang, C. Li, Q. Chen, Z. Hou, B. Xing, J. Lin, *Adv. Mater.* **2022**, *34*, 2106010; d) A. M. Cameron, A. Castoldi, D. E. Sanin, L. J. Flachsmann, C. S. Field, D. J. Puleston, R. L. Kyle, A. E. Patterson, F. Hässler, J. M. Buescher, B. Kelly, E. L. Pearce, E. J. Pearce, *Nat. Immun.* **2019**, *20*, 420.

[12] a) Y. Panahi, G. H. Alishiri, S. Parvin, A. Sahebkar, *J. Diet. Suppl.* **2016**, *13*, 209; b) Y. Sun, Z. Zuo, Y. Kuang, *Int. J. Mol. Sci.* **2020**, *21*, 8513; c) X. Li, X. Wang, Q. Liu, J. Yan, D. Pan, L. Wang, Y. Xu, F. Wang, Y. Liu, X. Li, M. Yang, *Adv. Healthcare Mater.* **2021**, *10*, 2100883; d) E. Rendra, V. Riabov, D. M. Mossel, T. Sevastyanova, M. C. Harmsen, J. Kzhyshkowska, *Immunobiology* **2019**, *224*, 242; e) G. Yang, J. S. Ni, Y. Li, M. Zha, Y. Tu, K. Li, *Angew. Chem., Int. Ed.* **2021**, *60*, 5386.

[13] a) F. Zhou, J. Mei, S. Yang, X. Han, H. Li, Z. Yu, H. Qiao, T. Tang, *ACS Appl. Mater. Interfaces* **2020**, *12*, 2009; b) H. Zhang, H. Xiong, W. Ahmed, Y. Yao, S. Wang, C. Fan, C. Gao, *Chem. Eng. J.* **2021**, *409*, 128147.

[14] a) Z. Lacza, E. Pankotai, A. Csordás, D. Gero, L. Kiss, E. M. Horváth, M. Kollai, D. W. Busija, C. Szabó, *Nitric Oxide* **2006**, *14*, 162; b) M. Zhao, Y. Wang, L. Li, S. Liu, C. Wang, Y. Yuan, G. Yang, Y. Chen, J. Cheng, Y. Lu, J. Liu, *Theranostics* **2021**, *11*, 1845; c) A. V. Kudryavtseva, G. S. Krasnov, A. A. Dmitriev, B. Y. Alekseev, O. L. Kardymon, A. F. Sadritdinova, M. S. Fedorova, A. V. Pokrovsky, N. V. Melnikova, A. D. Kaprin, A. A. Moskalev, A. V. Snezhkina, *Oncotarget* **2016**, *7*, 44879; d) F. J. Blanco, I. Rego, C. Ruiz-Romero, *Nat. Rev. Rheumatol.* **2011**, *7*, 161; e) E. T. Chouchani, V. R. Pell, E. Gaude, D. Aksentijević, S. Y. Sundier, E. L. Robb, A. Logan, S. M. Nadtochiy, E. N. J. Ord, A. C. Smith, F. Eyassu, R. Shirley, C. H. Hu, A. J. Dare, A. M. James, S. Rogatti, R. C. Hartley, S. Eaton, A. S. H. Costa, P. S. Brookes, S. M. Davidson, M. R. Duchen, K. Saeb-Parsy, M. J. Shattock, A. J. Robinson, L. M. Work, C. Frezza, T. Krieg, M. P. Murphy, *Nature* **2014**, *515*, 431.

[15] a) J. Yang, B. Ren, G. Yang, H. Wang, G. Chen, L. You, T. Zhang, Y. Zhao, *Cell Mol. Life Sci.* **2020**, *77*, 305; b) E. L. Mills, B. Kelly, L. A. J. O'Neill, *Nat. Immun.* **2017**, *18*, 488; c) M. M. Mehta, S. E. Weinberg, N. S. Chandel, *Nat. Rev. Immun.* **2017**, *17*, 608; d) Y. R. Zhang, J. Q. Luo, J. Y. Zhang, W. M. Miao, J. S. Wu, H. Huang, Q. S. Tong, S. Shen, K. W. Leong, J. Z. Du, J. Wang, *Small* **2020**, *16*, 2004240.

[16] a) R. Orihuela, C. A. McPherson, G. J. Harry, *Br. J. Pharmacol.* **2016**, *173*, 649; b) Y. Liu, X. Yuan, N. Muñoz, T. M. Logan, T. Ma, *Stem Cells Transl. Med.* **2019**, *8*, 93; c) Y. Zhang, S. Choksi, K. Chen, Y. Pobezinskaya, I. Linnoila, Z. G. Liu, *Cell Res.* **2013**, *23*, 898; d) S. Zanganeh, G. Hutter, R. Spitler, O. Lenkov, M. Mahmoudi, A. Shaw, J. S. Pajarinen, H. Nejadnik, S. Goodman, M. Moseley, L. M. Coussens, H. E. Daldrup-Link, *Nat. Nanotechnol.* **2016**, *11*, 986.

[17] a) T. Gaber, C. Strehl, F. Buttgereit, *Nat. Rev. Rheumatol.* **2017**, *13*, 267; b) N. A. Devanney, A. N. Stewart, J. C. Gensel, *Exp. Neurol.* **2020**, *329*, 113310; c) X. Chen, Z. Chen, B. Hu, P. Cai, S. Wang, S. Xiao, Y. Wu, X. Chen, *Small* **2018**, *14*, 1703164; d) J. Li, L. Zeng, Z. Wang, H. Chen, S. Fang, J. Wang, C. Cai, E. Xing, X. Liao, Z. Li, C. R. AshbyJr., Z. Chen, H. Chao, Y. Pan, *Adv. Mater.* **2022**, *34*, 2100245; e) F. Li, Y. Li, X. Yang, X. Han, Y. Jiao, T. Wei, D. Yang, H. Xu, G. Nie, *Angew. Chem., Int. Ed.* **2018**, *57*, 2377; f) J. Li, L. Xie, W. Sang, W. Li, G. Wang, J. Yan, Z. Zhang, H. Tian, Q. Fan, Y. Dai, *Angew. Chem., Int. Ed.* **2022**, *61*, e202200830.

[18] a) Y. Wang, N. Li, X. Zhang, T. Horng, *J. Biol. Chem.* **2021**, *297*, 100904; b) S. Jung, M. Choi, D. Ryu, H. Yi, S. Lee, J. Chang, H. Chung, Y. Kim, S. Kang, J. Lee, K. Kim, H. Kim, C. Kim, C. Lee, R. Williams, H. Kim, H. Lee, J. Auwerx, M. Shong, *Nat. Commun.* **2018**, *9*, 1551.

[19] J. Bossche, J. Baardman, N. Velden, A. Berg, R. Luque-Martin, H. Chen, M. Boshuizen, M. Ahmed, M. Hoeksema, A. Vos, M. Winther, *Cell Rep.* **2016**, *17*, 684.

[20] Y. Yuan, Y. Chen, T. Peng, L. Li, W. Zhu, F. Liu, S. Liu, X. An, R. Luo, J. Cheng, J. Liu, Y. Lu, *Clin. Sci.* **2019**, *133*, 1759.

[21] Z. Gao, Y. Li, F. Wang, T. Huang, K. Fan, Y. Zhang, J. Zhong, Q. Cao, T. Chao, J. Jia, S. Yang, L. Zhang, Y. Xiao, J.-Y. Zhou, X.-H. Feng, J. Jin, *Nat. Commun.* **2017**, *8*, 1805.

[22] E. L. Mills, L. A. O'Neill, *Eur. J. Immunol.* **2016**, *46*, 13.

[23] a) H. Yan, D. Shao, Y. H. Lao, M. Li, H. Hu, K. W. Leong, *Adv. Sci.* **2019**, *6*, 1900605; b) R. Li, Y. He, S. Zhang, J. Qin, J. Wang, *Acta. Pharm. Sin. B* **2018**, *8*, 14.

[24] a) Z. Tu, Y. Zhong, H. Hu, D. Shao, R. Haag, M. Schirner, J. Lee, B. Sullenger, K. W. Leong, *Nat. Rev. Mater.* **2022**, https://doi.org/10.1038/s41578-022-00426-z; b) H. Liang, B. Peng, C. Dong, L. Liu, J. Mao, S. Wei, X. Wang, H. Xu, J. Shen, H. Q. Mao, X. Gao, K. W. Leong, Y. Chen, *Nat. Commun.* **2018**, *9*, 4291; c) Y. Yang, L. Guo, Z. Wang, P. Liu, X. Liu, J. Ding, W. Zhou, *Biomaterials* **2021**, *264*, 120390; d) V. Chugh, K. Vijaya Krishna, A. Pandit, *ACS Nano* **2021**, *15*,17080.

[25] a) Q. Le, J. Lee, H. Lee, G. Shim, Y. Oh, *Acta Pharm. Sin. B* **2021**, *11*, 2096; b) Q. Xia, Y. Zhang, Z. Li, X. Hou, N. Feng, *Acta Pharm. Sin. B* **2019**, *9*, 675; c) M. Gao, C. Liang, X. Song, Q. Chen, Q. Jin, C. Wang, Z. Liu, *Adv. Mater.* **2017**, *29*, 1701429. d) L. Wang, X. Wang, F. Yang, Y. Liu, L. Meng, Y. Pang, M. Zhang, F. Chen, C. Pan, S. Lin, X. Zhu, K. W. Leong, J. Liu, *Nano Today* **2021**, *40*, 101280; e) Y. Miao, Y. Yang, L. Guo, M. Chen, X. Zhou, Y. Zhao, D. Nie, Y. Gan, X. Zhang, *ACS Nano* **2022**, *16*, 6527.

[26] a) N. Pishesha, A. M. Bilate, M. C. Wibowo, N. J. Huang, Z. Li, R. Deshycka, D. Bousbaine, H. Li, H. C. Patterson, S. K. Dougan, T. Maruyama, H. F. Lodish, H. L. Ploegh, *Proc. Natl. Acad. Sci. USA* **2017**, *114*, 3157; b) Q. Jiang, K. Wang, X. Zhang, B. Ouyang, H. Liu, Z. Pang, W. Yang, *Small* **2020**, *16*, 2001704; c) C. N. Morrell, H. Sun, A. M. Swaim, W. M. Baldwin Iii, *Am. J. Transplant.* **2007**, *7*, 2447.

[27] a) W. Liu, M. Zou, S. Qin, Y. Cheng, Y. Ma, Y. Sun, X. Zhang, *Adv. Funct. Mater.* **2020**, *30*, 2003559; b) Z. He, Y. Zhang, N. Feng, *Mater. Sci. Eng., C* **2020**, *106*, 110298.

[28] a) C. Xu, Y. Jiang, Y. Han, K. Pu, R. Zhang, *Adv. Mater.* **2021**, *33*, 2008061; b) J. Li, X. Jiang, H. Li, M. Gelinsky, Z. Gu, *Adv. Mater.* **2021**, *33*, 2004172.

[29] a) Y. Jiang, N. Krishnan, J. Zhou, S. Chekuri, X. Wei, A. V. Kroll, C. L. Yu, Y. Duan, W. Gao, R. H. Fang, L. Zhang, *Adv. Mater.* **2020**,

32, 2001808; b) L. Rao, L. Bu, B. Cai, J. Xu, A. Li, W. Zhang, Z. Sun, S. Guo, W. Liu, T. Wang, X. Zhao, *Adv. Mater.* **2016**, *28*, 3460; c) R. H. Fang, A. V. Kroll, W. Gao, L. Zhang, *Adv. Mater.* **2018**, *30*, 1706759.

[30] a) F. Iannone, G. Lapadula, *Aging: Clin. Exp. Res.* **2003**, *15*, 364; b) J. Yu, P. Cai, X. Zhang, T. Zhao, L. Liang, S. Zhang, H. Liu, X. Chen, *ACS Nano* **2021**, *15*, 7618.

[31] L. Rao, S. Zhao, C. Wen, R. Tian, L. Lin, B. Cai, Y. Sun, F. Kang, Z. Yang, L. He, J. Mu, Q. Meng, G. Yao, N. Xie, X. Chen, *Adv. Mater.* **2020**, *32*, 2004853.

[32] a) S. Zou, B. Wang, C. Wang, Q. Wang, L. Zhang, *Nanomedicine.* **2020**, *15*, 625; b) P. Dash, A. M. Piras, M. Dash, *J. Controlled Release* **2020**, *327*, 546.

[33] D. G. You, G. T. Lim, S. Kwon, W. Um, B. H. Oh, S. H. Song, J. Lee, D. G. Jo, Y. W. Cho, J. H. Park, *Sci. Adv.* **2021**, *7*, eabe0083.

[34] C. Ren, D. Li, Q. Zhou, X. Hu, *Biomaterials* **2020**, *232*, 119752.

[35] a) J. Wang, Y. Zhao, W. Wang, Z. Du, D. Yan, C. Li, Z. Chen, *Cell. Physiol. Biochem.* **2013**, *32*, 121; b) S. Onuora, *Nat. Rev. Rheumatol.* **2016**, *12*, 313.

[36] H. Zhang, C. Lin, C. Zeng, Z. Wang, H. Wang, J. Lu, X. Liu, Y. Shao, C. Zhao, J. Pan, S. Xu, Y. Zhang, D. Xie, D. Cai, X. Bai, *Ann. Rheum. Dis.* **2018**, *77*, 1524.

[37] B. A. Payne, I. J. Wilson, C. A. Hateley, R. Horvath, M. Santibanez-Koref, D. C. Samuels, D. A. Price, P. F. Chinnery, *Nat. Genet.* **2011**, *43*, 806.

[38] a) M. Johnson, C. N. Mowa, *Cell Tissue Res.* **2021**, *384*, 771; b) Y. Zhou, G. Wang, P. Wang, Z. Li, T. Yue, J. Wang, P. Zou, *Angew. Chem., Int. Ed.* **2019**, *58*, 11763.

[39] X. Wang, Y. Ning, P. Zhang, B. Poulet, R. Huang, Y. Gong, M. Hu, C. Li, R. Zhou, M. J. Lammi, X. Guo, *Cell Death Dis.* **2021**, *12*, 551.

[40] J. Purhonen, V. Grigorjev, R. Ekiert, N. Aho, J. Rajendran, R. Pietras, K. Truvé, M. Wikström, V. Sharma, A. Osyczka, V. Fellman, J. Kallijärvi, *Nat. Commun.* **2020**, *11*, 322.

[41] V. Lo Faro, I. M. Nolte, J. B. Ten Brink, H. Snieder, N. M. Jansonius, A. A. Bergen, *Front. Genet.* **2021**, *12*, 781189.

[42] a) Y. Liu, Y. Zhao, R. Tang, X. Jiang, Y. Wang, T. Gu, *Mol. Med. Rep.* **2020**, *22*, 5105; b) I. Duroux-Richard, F. Apparailly, M. Khoury, *Front. Physiol.* **2021**, *12*, 738140; c) S. Li, H. Pan, C. Tan, Y. Sun, Y. Song, X. Zhang, W. Yang, X. Wang, D. Li, Y. Dai, Q. Ma, C. Xu, X. Zhu, L. Kang, Y. Fu, X. Xu, J. Shu, N. Zhou, F. Han, D. Qin, W. Huang, Z. Liu, Q. Yan, *Stem Cell Rep.* **2018**, *10*, 808.

[43] J. Willemsen, M. T. Neuhoff, T. Hoyler, E. Noir, C. Tessier, S. Sarret, T. N. Thorsen, A. Littlewood-Evans, J. Zhang, M. Hasan, J. S. Rush, D. Guerini, R. M. Siegel, *Cell Rep.* **2021**, *37*, 109977.

[44] E. M. De Francesco, G. Bonuccelli, M. Maggiolini, F. Sotgia, M. P. Lisanti, *Oncotarget* **2017**, *8*, 67269.

[45] J. Iske, M. Seyda, T. Heinbokel, R. Maenosono, K. Minami, Y. Nian, M. Quante, C. S. Falk, H. Azuma, F. Martin, J. F. Passos, C. U. Niemann, T. Tchkonia, J. L. Kirkland, A. Elkhal, S. G. Tullius, *Nat. Commun.* **2020**, *11*, 4289.

[46] a) M. de Gaetano, D. Crean, M. Barry, O. Belton, *Front. Immunol.* **2016**, *7*, 275; b) Z. Xu, L. Xu, W. Li, X. Jin, X. Song, X. Chen, J. Zhu, S. Zhou, Y. Li, W. Zhang, X. Dong, X. Yang, F. Liu, H. Bai, Q. Chen, C. Su, *Nat. Commun.* **2017**, *8*, 16035.

[47] H. Semba, N. Takeda, T. Isagawa, Y. Sugiura, K. Honda, M. Wake, H. Miyazawa, Y. Yamaguchi, M. Miura, D. M. Jenkins, H. Choi, J. W. Kim, M. Asagiri, A. S. Cowburn, H. Abe, K. Soma, K. Koyama, M. Katoh, K. Sayama, N. Goda, R. S. Johnson, I. Manabe, R. Nagai, I. Komuro, *Nat. Commun.* **2016**, *7*, 11635.

[48] a) W. Liu, X. Duan, X. Fang, W. Shang, C. Tong, *Autophagy* **2018**, *14*, 1293; b) T. Lima, T. Y. Li, A. Mottis, J. Auwerx, *Nat. Aging* **2022**, *2*, 199.

[49] J. Goldberg, A. Currais, M. Prior, W. Fischer, C. Chiruta, E. Ratliff, D. Daugherty, R. Dargusch, K. Finley, P. B. Esparza-Moltó, J. M. Cuezva, P. Maher, M. Petrascheck, D. Schubert, *Aging Cell* **2018**, *17*, e12715.

[50] D. Nolfi-Donegan, A. Braganza, S. Shiva, *Redox Biol.* **2020**, *37*, 101674.

[51] J. Qing, Z. Zhang, P. Novák, G. Zhao, K. Yin, *Acta Biochim. Biophys. Sin.* **2020**, *52*, 917.

[52] T. Saitoh, M. Igura, T. Obita, T. Ose, R. Kojima, K. Maenaka, T. Endo, D. Kohda, *EMBO J.* **2007**, *26*, 4777.

[53] a) B. R. Gauthier, A. Wiederkehr, M. Baquié, C. Dai, A. C. Powers, J. Kerr-Conte, F. Pattou, R. J. MacDonald, J. Ferrer, C. B. Wollheim, *Cell Metab.* **2009**, *10*, 110; b) P. Huangyang, F. Li, P. Lee, I. Nissim, A. M. Weljie, A. Mancuso, B. Li, B. Keith, S. S. Yoon, M. C. Simon, *Cell Metab.* **2020**, *31*, 174.

[54] C. Gao, Q. Huang, C. Liu, C. H. T. Kwong, L. Yue, J. B. Wan, S. M. Y. Lee, R. Wang, *Nat. Commun.* **2020**, *11*, 2622.

[55] a) Y. Han, C. Gao, H. Wang, J. Sun, M. Liang, Y. Feng, Q. Liu, S. Fu, L. Cui, C. Gao, Y. Li, Y. Yang, B. Sun, *Bioact. Mater.* **2021**, *6*, 529; b) Y. Zhang, K. Cai, C. Li, Q. Guo, Q. Chen, X. He, L. Liu, Y. Zhang, Y. Lu, X. Chen, T. Sun, Y. Huang, J. Cheng, C. Jiang, *Nano Lett.* **2018**, *18*, 1908.

[56] a) A. Hartnell, J. Steel, H. Turley, M. Jones, D. G. Jackson, P. R. Crocker, *Blood* **2001**, *97*, 288; b) M. S. Macauley, P. R. Crocker, J. C. Paulson, *Nat. Rev. Immunol.* **2014**, *14*, 653.

[57] a) D. A. Murphy, H. Cheng, T. Yang, X. Yan, I. M. Adjei, *Mol. Pharmaceutics* **2021**, *18*, 2935; b) M. Song, T. Liu, C. Shi, X. Zhang, X. Chen, *ACS Nano* **2016**, *10*, 633.

[58] a) J. Mosafer, M. Teymouri, *Nanomed. Biotechnol.* **2018**, *46*, 1146; b) J. Koerner, D. Horvath, V. L. Herrmann, A. MacKerracher, B. Gander, H. Yagita, J. Rohayem, M. Groettrup, *Nat. Commun.* **2021**, *12*, 2935.